

Adaptive Kalman Filter-based Estimator with Sea Trail Data to Calculate Ship States in Complex Navigation Conditions

Yufei Wang¹, Lokukaluge P. Perera^{1,2}, and Bjørn-Morten Batalden¹

¹UiT The Arctic University of Norway, Tromsø, Norway

²SINTEF Digital, SINTEF AS, Oslo, Norway

ABSTRACT

With the progress of innovative technologies, ships in future with different autonomy levels are anticipated to enter the realm of maritime transportation. As a result, the scenarios of multi-ship encounters at sea can become more complex and the risk of potential collisions can be difficult to elevate. To support navigation safety and guarantee the required situation awareness level, it is therefore essential to acquire ship navigation states with a greater degree of precision. The Kalman Filter (KF)-based techniques are one of the popular approaches for deriving the ship navigation state by merging the prior estimates from physics-based models with measurements from onboard sensors. However, many KF-based estimates are calculated by assuming constant system and measurement uncertainties during the iterative process. In this study, an adaptive tuning mechanism in the KF-based techniques is utilized to estimate ship navigation states. This approach enables the estimation processes to skillfully reduce both system and measurement noises estimations. Consequently, it results in the generation of smoother and more responsive estimates of the respective vessel states, particularly when confronted with variations in rudder orders or encountering abnormal measured positions.

KEY WORDS: State estimation; Kalman Filter (KF); Unscented Kalman Filter (UKF); Kinematic motion model; Adaptive tuning mechanism; Gaussian Process Regression.

INTRODUCTION

Autonomous shipping is expected to exist and show its benefits in maritime transportation in the coming future. With respect to the current development of autonomous ships, onboard sensors are considered as one of the fundamental parts (Perera, 2019;Thombre et al., 2022). These sensors are specifically designed to provide digital navigators of

autonomous ships with precise navigation information, ensuring the maintenance of adequate situation awareness. Since not all ship navigation information can be directly measured, and the measurements from sensors may contain measurement noise, it is generally considered to implement KF-based techniques to generate estimated states with higher precision.

Given the convenience of kinematic motion models, using KF-based estimation combined with these models is a favorable choice (Li and Jilkov, 2003). One advantage of employing kinematic motion models is the ignorance of hydrodynamic coefficients which are associated with external forces and moments. The influences of external disturbances can be modeled as system noises in kinematic motion models. The curvilinear motion model (CMM) and the constant turn rate and acceleration model (CTRA) represent two kinematic motion models which can encompass diverse motions exhibited by ships. As a result, these models are widely employed in numerous research studies to provide essential ship navigation states (Perera, 2017;Wang et al., 2023). Nevertheless, it is important to recognize that these kinematic motion models operate under the assumption of constant accelerations and turn rates. Clearly, this assumption becomes invalid when ships execute new rudder orders or adjust engine power. Consequently, the utilization of constant system noises in the CMM and CTRA within the KF-based estimation can lead to less precise estimates. Another crucial factor to consider is the potential for measurement bias when utilizing GNSS systems. To enhance measurement precision, the augmentation of GNSS is actively encouraged. However, it is important to note that while such augmentation can improve precision, it does not guarantee the elimination of measure abnormalities (Baybura et al., 2019). When the measured outliers exceed certain thresholds, the KF-based estimation may yield questionable results.

Therefore, from a practical perspective, the application of KF-based techniques should incorporate adaptive tuning of system and

measurement noises to enhance robustness. This adjustment ensures that the filtering process remains resilient to varying conditions, contributing to more reliable and precise state estimates.

Adaptive filtering

There are several approaches which are used for tuning system and measurement noises adaptively. The first approach involves a statistical analysis of the innovation (Hu et al., 2003). In the KF-based techniques, the innovation is the difference between the observed measurements and the prior estimates. Through an examination of the statistical properties of innovations, one can assess the evolving characteristics of the associated system and measurement noises over time. An alternative adaptive approach utilizes the innovation as a criterion to identify the occurrence of new maneuvers of ships. When new maneuvers are identified, a scale factor is employed to adjust the system noises (Efe et al., 1999; Almagbile et al., 2010). Instead of the scale factor, there are studies which introduce the forgetting factor with a comparable function for adjusting system noises (Ohhira et al., 2021; Wu et al., 2021). There are also proposed approach which contains multiple models, such as Interacting Multiple Models (IMM) and Multiple Model Adaptive Estimation (MMAE) (Mazor et al., 1998; Alsuwaidan et al., 2011). These methods incorporate multiple models to account for system uncertainties. IMM employs an interaction mechanism facilitating seamless transitions between different models based on measurements. In contrast, MMAE is designed to dynamically select the most suitable model from a set of candidates, adapting to the evolving characteristics of measurements.

In the first category of methods, the accurate determination of the statistical properties of innovation necessitates the specification of the quantity of historical data. An analysis relying on a smaller dataset may fail to accurately reflect the proper statistical properties, while an analysis utilizing a larger dataset runs the risk of averaging out these statistical properties. Within the second category of methods, the determination of both the scale factors and forgetting factors needs to be done artificially. Furthermore, it is essential to explore multiple factors associated with optimal maneuver fits in advance. Concerning IMM and MMAE, a significant portion of the computational cost is allocated to identifying the most suitable models. The MMAE may struggle in situations where there is uncertainty or ambiguity in the selection of appropriate models, which can impact its overall performance. The IMM is sensitive to model switching so that incorrect model switching decisions can happen in rapidly changing or unpredictable environments. It is worth noting that models which can be utilized in the IMM framework must share identical system states. This constraint serves as a limitation when employing the IMM.

In this study, an adaptive tuning mechanism is designed for ship navigation state estimation using KF-based techniques and kinematic motion models. The design takes into account that ships, often of substantial tonnage, primarily undergo maneuvers triggered by different rudder orders rather than changes in engine states. Considering measurements obtained from onboard sensors, the adaptive tuning mechanism primarily focuses on outliers in GNSS measurements. This is rational as the precision of GNSS measurements relies on the operational status of satellites and ground equipment, factors not under the control of ships. Therefore, the proposed adaptive tuning mechanism for ship maneuvers primarily deals with two scenarios: new rudder orders and abnormal GNSS measurements.

The paper follows a structured outline. The next section, Preliminaries, encompasses all the methods employed in this study. Subsequently, the Simulation and Experiment Setup section makes a brief presentation of the simulated and sea-trial experiments. This is succeeded by the

presentation of Experiment Results and Related Discussions. The section of Conclusions is in the last.

METHODOLOGY

Kinematic motion models

Three kinematic motion models will be used to describe the ship maneuvers—the Constant Angular Acceleration (CAA) model, the Curvilinear motion model (CMM), and the Constant Turn Rate & Acceleration (CTRA) model. The states described by these models are illustrated in Fig.1. The onboard sensors, including the GNSS, gyroscope, and IMU, are assumed to be positioned at the geometric center of the ship, denoted as point C. The acquired measurements include the UTM coordinates of C (Z_{NC}, Z_{EC}), ship's true heading (z_{ψ_T}), turn rate (z_r), and the accelerations in the vessel body reference frame (Z_{aw}, Z_{av}). It is essential to highlight that, as the measured position is converted into UTM coordinates, the heading utilized in the CMM and CTRA is adjusted to align with grid north ψ_G . Given that the measured heading ψ_T is in true north, a deviation which is denoted as grid convergence γ can exist. Specific corrections are necessary, and details on correction methods can be found in (Kawase, 2013).

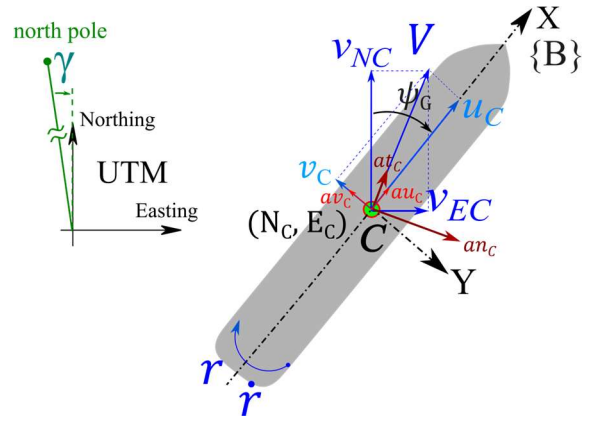


Fig.1. States used in the CAA, CMM, and CTRA. Onboard sensors (GNSS, gyroscope, and IMU) are installed in C.

The system and measurement models of the utilized kinematic motion models are listed in Tab.1-3. In the KF-based state estimation, the CAA is initially executed to generate estimated values for heading, turn rate, and angular acceleration. These estimates are then utilized as parameters in the CMM and CTRA (Eq.4-6). It is crucial to emphasize that the kinematic motion models are constructed on the assumption of constant accelerations and turn rates. When the ship adopts new rudder orders, these assumptions are no longer valid. Consequently, the uncertainties w_x and w_z must be adaptively reevaluated to ensure enhanced estimation precision. As w_x and w_y is assumed to be white Gaussian noises, the covariance matrix Q and R are thus needs to be adaptively assigned.

Table 1:

CAA:	$x(t) = [\psi_T, r, \dot{r}]^T$; $z[t_k] = [z_{\psi_T}, z_r]$
system model:	$\dot{x}(t) = \begin{bmatrix} 0 & 1 & 0 \\ 0 & 0 & 1 \\ 0 & 0 & 0 \end{bmatrix} \cdot x(t) + w_x \quad (1)$ $(w_x \sim \mathcal{N}(0, Q \in \mathbb{R}^{3 \times 3}))$
measurement model:	$z[t_k] = \begin{bmatrix} 1 & 0 & 0 \\ 0 & 1 & 0 \end{bmatrix} x[t_k] + w_z \quad (2)$ $(w_z \sim \mathcal{N}(0, R \in \mathbb{R}^{2 \times 2}))$

Table 2:

CMM:	$\mathbf{x}(t) = [N_C, E_C, v_{NC}, v_{EC}, at_c, an_c]^T$ $\mathbf{z}[t_k] = [Z_{NC}, Z_{EC}, z_{au}, z_{av}]$
system model:	$\dot{\mathbf{x}}(t) = \begin{bmatrix} v_{NC} \\ v_{EC} \\ at_c f^{v_{NC}} - an_c f^{v_{EC}} \\ at_c f^{v_{EC}} + an_c f^{v_{NC}} \\ 0 \\ 0 \end{bmatrix} + \mathbf{w}_x \quad (3)$ <p style="text-align: center;">$(\mathbf{w}_x \sim \mathcal{N}(\mathbf{0}, \mathbf{Q} \in \mathbb{R}^{6 \times 6}))$</p> $f^{v_{NC}} = \frac{v_{NC}}{V}, f^{v_{EC}} = \frac{v_{EC}}{V} \quad \left(V = \sqrt{v_{NC}^2 + v_{EC}^2} \right)$
measurement model:	$\mathbf{z}[t_k] = \begin{bmatrix} Z_{NC} \\ Z_{EC} \\ h_1 \cos(\psi_G) + h_2 \sin(\psi_G) \\ h_1 \cos(\psi_G) - h_2 \sin(\psi_G) \end{bmatrix} + \mathbf{w}_z \quad (4)$ <p style="text-align: center;">$(\mathbf{w}_z \sim \mathcal{N}(\mathbf{0}, \mathbf{R} \in \mathbb{R}^{4 \times 4}))$</p> $h_1 = at_c f^{v_{NC}} - an_c f^{v_{EC}} + r v_{EC}$ $h_2 = at_c f^{v_{EC}} + an_c f^{v_{NC}} - r v_{NC}$

Table 3:

CTRA:	$\mathbf{x}(t) = [N_C, E_C, u_C, v_C, au_C, av_C]^T$ $\mathbf{z}[t_k] = [Z_{NC}, Z_{EC}, z_{au}, z_{av}]$
system model:	$\dot{\mathbf{x}}(t) = \begin{bmatrix} u_C \cos(\psi_G) - v_C \sin(\psi_G) \\ v_C \cos(\psi_G) + u_C \sin(\psi_G) \\ au_C \\ av_C \\ 0 \\ 0 \end{bmatrix} + \mathbf{w}_x \quad (5)$ <p style="text-align: center;">$(\mathbf{w}_x \sim \mathcal{N}(\mathbf{0}, \mathbf{Q} \in \mathbb{R}^{6 \times 6}))$</p>
measurement model:	$\mathbf{z}[t_k] = \begin{bmatrix} Z_{NC} \\ Z_{EC} \\ z_{au} - v_C r \\ z_{av} + u_C r \end{bmatrix} + \mathbf{w}_z \quad (6)$ <p style="text-align: center;">$(\mathbf{w}_z \sim \mathcal{N}(\mathbf{0}, \mathbf{R} \in \mathbb{R}^{4 \times 4}))$</p>

KF-based state estimation

It is evident that CAA and CTRA are linear models, while CMM is nonlinear. In this study, the KF is employed for estimating states in CAA and CTRA, and the UKF is utilized in CMM for estimating related states. As the system models are described in continuous-time, the KF-based estimation requires the implementation of numerical solutions for the corresponding continuous-time differential equations. The algorithms for KF and UKF are presented in Fig.2 and 3. These algorithms are based on the constant \mathbf{Q} and \mathbf{R} which required to be initialized in the initialization stage.

In the execution of the KF-based estimation, the states in the CAA will be estimated firstly. This is attributed to the fact that the innovation of the turn rate in the CAA (y_r) can be employed as the criterion to assess whether the ship maintains a constant turn rate. A variation in the turn rate is anticipated to result in altered values of y_r . When deviated values of y_r are identified, \mathbf{Q} in the CMM and CTRA will be increased by multiplying it with a scale factor α . The establishment of a relationship between y_r and α is essential. Details of this relationship will be elaborated upon in the following subsection.

Regarding \mathbf{R} in the CMM and CTRA, the innovations of the position, denoted as y_N and y_E , are employed to identify potential biases in the measured positions (Fig.4). If the innovation exceeds a predefined threshold, a substantial scaling factor is implemented on \mathbf{R} , prioritizing the computation of the Kalman gain. The threshold is determined through GNSS testing. In this study, the threshold is set to 2 [m] and a scaling factor of 1000 will be multiplied to \mathbf{R} if the innovations are larger than the threshold. It is important to note that the assumption is made

that abnormal data from the GNSS occur infrequently, typically during short navigation periods. The occurrence of abnormal GNSS data over an extended period could lead to issues in inertial navigation, which is beyond the scope of this paper.

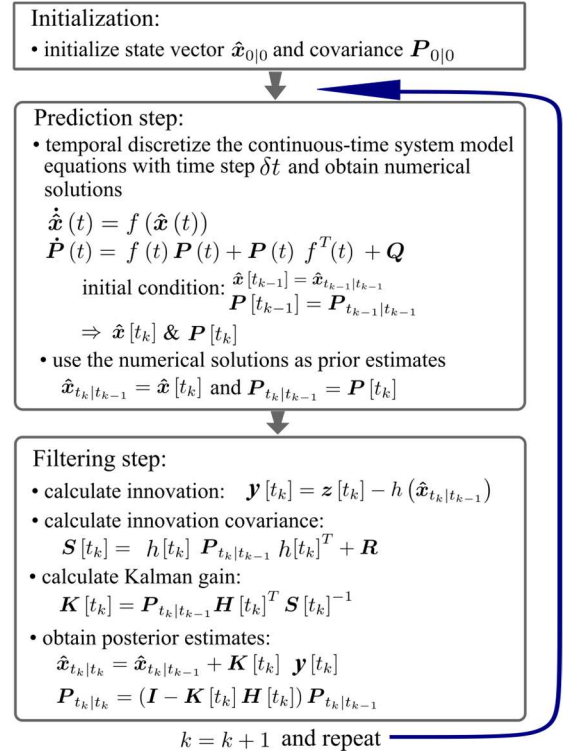


Fig. 2. KF algorithm (used for the CAA and CTRA)

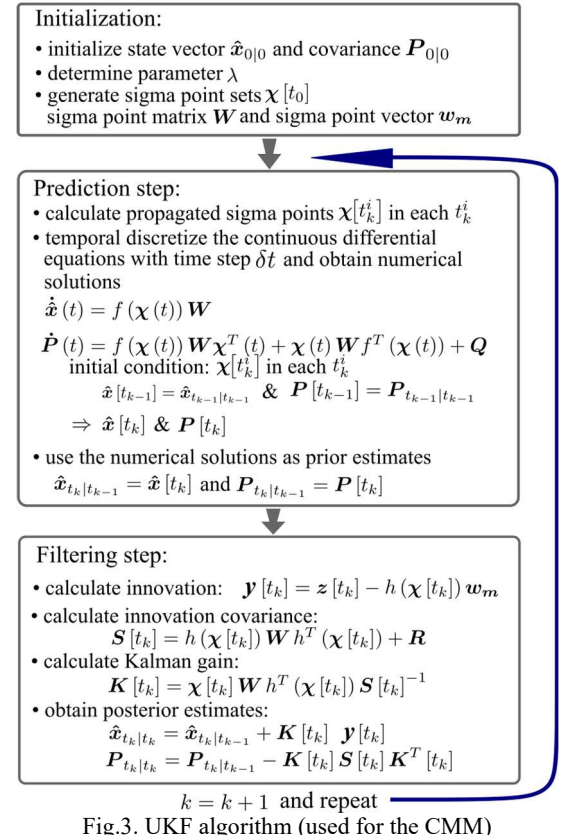


Fig.3. UKF algorithm (used for the CMM)

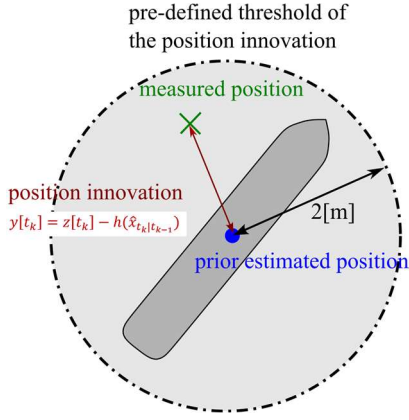


Fig.4. The measurement noise \mathbf{R} will be modified if position innovations are outside the colored circle that is regulated by a pre-defined threshold.

Gaussian process regression in adaptive tuning

Gaussian process regression (GPR) is widely utilized in machine learning and statistical analysis. GPR models demonstrate exceptional proficiency in capturing complex relationships within datasets, drawing on foundational principles rooted in probability theory. For an input with arbitrary N samples $(\mathbf{x}_1, \mathbf{x}_2, \dots, \mathbf{x}_N)$, if the corresponding output $\mathbf{f} = (f(\mathbf{x}_1), f(\mathbf{x}_2), \dots, f(\mathbf{x}_N))$ follows a multiple Gaussian distribution $\mathcal{N}(\boldsymbol{\mu}, \mathbf{K})$, it can be defined that \mathbf{f} follows a Gaussian process:

$$\mathbf{f} \sim GP(\boldsymbol{\mu}, \mathbf{K}) \quad (7)$$

where $\boldsymbol{\mu} = (\mu(\mathbf{x}_1), \mu(\mathbf{x}_2), \dots, \mu(\mathbf{x}_N))$, $K_{nn'} = k(\mathbf{x}_n, \mathbf{x}_{n'})$.

In many cases, through suitable data transformations, it is often feasible to assume $\boldsymbol{\mu}$ as 0, making the explicit modeling of $\boldsymbol{\mu}$ unnecessary. The elements $K_{nn'}$ in the covariance matrix \mathbf{K} are referred to as the kernel function. This function possesses the property that if two inputs exhibit similarity, the corresponding element in the matrix will have a higher value. In this study, the squared exponential kernel function is used (Eq.8).

$$k(\mathbf{x}_n, \mathbf{x}_{n'} | \boldsymbol{\theta}) = \theta_1 \exp\left(-\frac{(\mathbf{x}_n - \mathbf{x}_{n'})^T (\mathbf{x}_n - \mathbf{x}_{n'})}{2\theta_2}\right) + \theta_3 \delta(\mathbf{x}_n, \mathbf{x}_{n'}) \quad (8)$$

where δ is the Kronecker-delta.

Given the known datasets $\mathcal{D} = \{(x_1, y_1), \dots, (x_N, y_N)\}$, if the function \mathbf{f} which satisfies $\mathbf{y} = \mathbf{f}(\mathbf{x})$ is generated by $GP(0, k(\mathbf{x}_n, \mathbf{x}_{n'}))$, the output of a unknown input x^* can be also represented by a Gaussian distribution (Eq.9).

$$p(y^* | x^*, \mathcal{D}) = \mathcal{N}\left(k_*^T K^{-1} y, k_{**} - k_*^T K^{-1} k_*\right) \quad (9)$$

where: $k_* = k(\mathbf{x}_n, x^* | \boldsymbol{\theta})$, $k_{**} = k(x^*, x^* | \boldsymbol{\theta})$

Based on Eq.9, the expectation of y^* is equal to $k_*^T K^{-1} y$. It should be noted that Eq.9 only covers the case where the input x^* is single, which is the primary focus of this study. However, it is worth mentioning that GPR is also applicable to scenarios involving multiple unknown inputs.

Another task involving the utilization of GPR is the determination of the hyperparameter $\boldsymbol{\theta}$. Given that the elements $k(\mathbf{x}_n, \mathbf{x}_{n'} | \boldsymbol{\theta})$ are influenced by $\boldsymbol{\theta}$, the matrix \mathbf{K} is consequently dependent on $\boldsymbol{\theta}$. In this scenario, the

probability of y based on dataset \mathcal{D} can be expressed as:

$$p(y | \mathcal{D}) = \mathcal{N}(y | 0, K_{\boldsymbol{\theta}}) = \frac{1}{(2\pi)^{N/2}} \frac{1}{|K_{\boldsymbol{\theta}}|^{1/2}} \exp\left(-\frac{1}{2} y^T K_{\boldsymbol{\theta}}^{-1} y\right) \quad (10)$$

The method of maximum likelihood estimation can be employed to determine $\boldsymbol{\theta}$. The logarithm of $p(y | \mathcal{D})$ can be expressed as:

$$L = \log p(y | \mathcal{D}) \propto -\log |K_{\boldsymbol{\theta}}| - y^T K_{\boldsymbol{\theta}}^{-1} y + \text{const} \quad (11)$$

with:

$$\frac{\partial L}{\partial \boldsymbol{\theta}} = \frac{\partial L}{\partial K_{\boldsymbol{\theta}}} \frac{\partial K_{\boldsymbol{\theta}}}{\partial \boldsymbol{\theta}} = -\text{tr}\left(K_{\boldsymbol{\theta}}^{-1} \frac{\partial K_{\boldsymbol{\theta}}}{\partial \boldsymbol{\theta}}\right) + (K_{\boldsymbol{\theta}}^{-1} y)^T \frac{\partial K_{\boldsymbol{\theta}}}{\partial \boldsymbol{\theta}} (K_{\boldsymbol{\theta}}^{-1} y) \quad (12)$$

Utilizing the gradient of L (Eq.12), optimization algorithms can be applied to estimate $\boldsymbol{\theta}$. In this study, the L-BFGS algorithm is chosen to compute $\boldsymbol{\theta}$, and further details about this algorithm can be found in (Andrew and Gao, 2007).

In this study, the absolute value of the innovation of turn rate $|y_r|$ and the optimally-fitted scaling factor α undergo initial testing through simulated maneuvers in the UiT bridge simulator. The training dataset is consequently formed by pairs of $|y_r|$ and α . Figure 5 illustrates the comprehensive workflow of the proposed adaptive tuning mechanism. In each iteration, $|y_r|$ from the CAA is employed in the trained GPR model to dynamically determine α . The system noise \mathbf{Q} is consequently modified by α , resulting in \mathbf{Q}^* in the CMM and CTRA. Concurrently, the innovations y_N and y_E from the CMM and CTRA are utilized to assess whether the measured positions exhibit abnormal behavior. When abnormalities are detected, \mathbf{R} is substituted with \mathbf{R}^* to ensure that the filters reduce the emphasis on the measured data.

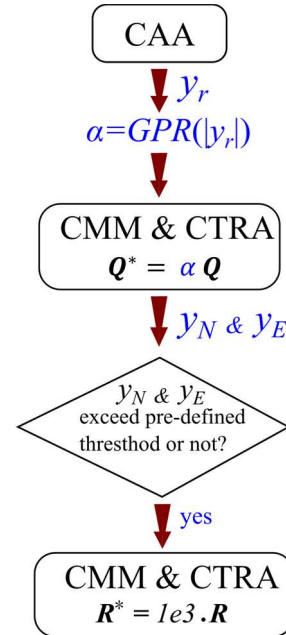


Fig.5. The workflow of the proposed adaptive tuning mechanism

EXPERIMENT PREPARATION

In this study, both simulated and sea-trial experiments will be conducted to validate the adaptive tuning mechanism. The simulated experiment takes place in the UiT bridge simulator (Fig.6).



Fig.6. UiT bridge simulator and the execution of simulated maneuvers

The sea-trial experiment is conducted using the UiT autonomous ship named "Ymir" in the Tromsø area (Fig.7). The ship is equipped with a variety of sensors, and a specialized data collection platform is designed to acquire the necessary measurements from selected sensors.



Fig.7. The equipped sensors in the autonomous ship "Ymir" and the sea trail experiment in Tromsø area.

Training data sets

During simulated maneuvers, the actual ship navigation states can be obtained directly from the simulator. Consequently, the optimal α with respect to $|y_r|$ can be determined through multiple offline trials. It is noteworthy that one of the advantages of employing GPR is that it does not necessitate an excessive number of experimental trials, implying significant cost savings. The training data sets are obtained from a simulated maneuver which contains straight line, starboard turning, and port turning. In Fig.8, it can be observed that $|y_r|$ have significant change in several time steps which imply that the ship has a new rudder order in the related steps. The innovation is further categorized into four groups by different levels of values.

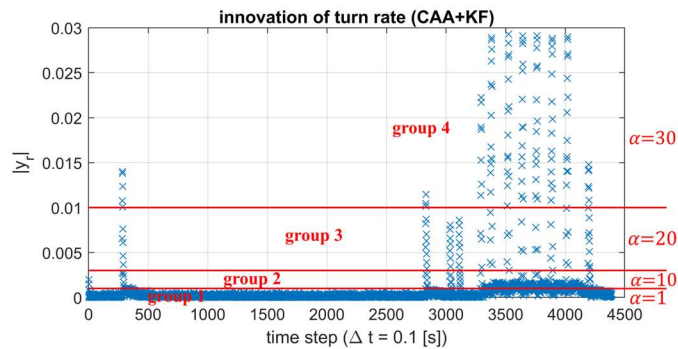


Fig.8. The absolute value of innovation of turn rate from the CAA. The maneuver is executed in the UiT bridge simulator. The $|y_r|$ values are categorized into four distinct groups, each assigned with an optimal α .

The training dataset \mathcal{D} is randomly chosen from the four groups, with a slightly greater number of samples from groups exhibiting a larger range

of (Fig.9). Artificial noises are introduced to each group's optimal α . The introduction of artificial noises has a negligible impact on estimation precision, yet it plays a role in enhancing the fitting within the Gaussian process.

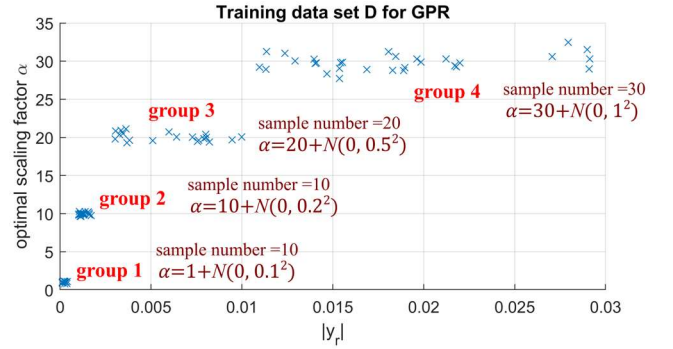


Fig.9. Sampled data set \mathcal{D} used for the training of GPR. Noted that the values of the optimal α in each group are added with artificial white Gaussian noises.

RESULTS AND DISCUSSIONS

Parameters initialization.

The parameters requiring initialization are outlined in Tab.4. The initial values for \mathbf{Q} in all kinematic motion models are optimized for straight-line maneuvers, while the initialization of \mathbf{R} is based on the sensors' performance characteristics. For the numerical solution in both the KF and UKF, the second-order Runge–Kutta explicit method is employed with a discretized time step δt .

Table.4. initialized parameters used in the KF-based estimation

parameters	value
dt	0.13[s] (time interval between consecutive measurements)
δt	0.0065 [s] (time interval used in temporal discretization)
\mathbf{Q} (CAA)	$diag\left(\left(\frac{0.1\pi}{180}\right)^2, \left(\frac{0.01\pi}{180}\right)^2, \left(\frac{0.001\pi}{180}\right)^2\right)$
\mathbf{Q} (CMM)	$diag(1^2, 1^2, 0.5^2, 0.5^2, 0.25^2, 0.25^2)$
\mathbf{Q} (CTRA)	$diag(0.3^2, 0.3^2, 0.1^2, 0.1^2, 0.03^2, 0.03^2)$
\mathbf{R} (CAA)	$diag\left(\left(\frac{0.5\pi}{180}\right)^2, \left(\frac{0.01\pi}{180}\right)^2\right)$
\mathbf{R} (CMM)	$diag(1^2, 1^2, 0.01^2, 0.01^2)$
\mathbf{R} (CTRA)	$diag(1^2, 1^2, 0.01^2, 0.01^2)$
λ	1.72 (unscented transform parameter used in the UKF)
θ	$(\theta_1, \theta_2, \theta_3) = (0.2, 0.4, 0.15)$ (hyperparameters in the kernel function)

Gaussian Process Regression Training

The regression outcome derived from the data set \mathcal{D} is illustrated in Fig.10. The red solid line depicts the expected values of predicted α across a range of 300 $|y_r|$, spanning from 0 to 0.03. The plot also includes 95% prediction intervals. Following training, the optimal θ is determined to be (0.0023, 8.7554, 0.7914). It is noticeable that the predicted α exhibits a gradual increase between distinct groups, with the predicted values in group 3 and group 4 displaying linear distributions.

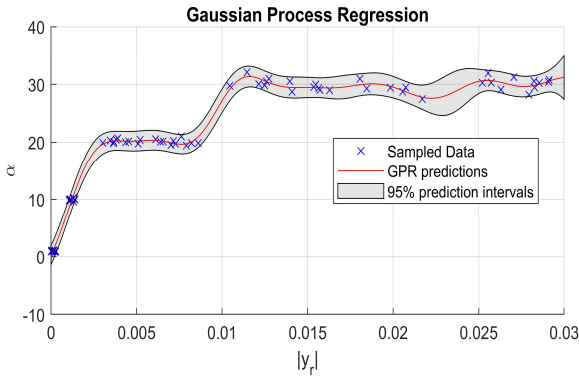


Fig.10. The predicted scaling factor α with the sampled data sets \mathcal{D} from the simulated maneuver.

State estimation with sea-trail data

Two maneuvers conducted by "Ymir" serve as the basis for evaluating the proposed adaptive tuning mechanism. These maneuvers encompass a zigzag and a port-turning maneuver, with Fig.11 illustrating the measured positions during these maneuvers. Notably, during the port-turning maneuver, unusual measurements become evident as the ship undergoes the turning phase, with recorded positions remaining static for several seconds. Due to the absence of actual true data from sea-trial experiments, innovations are employed to assess the estimation performances of the CMM and CTRA. Large values of innovations can suggest a suboptimal fit or model inaccuracies. Therefore, it is anticipated that the innovations should be maintained on a small scale for precise estimation.

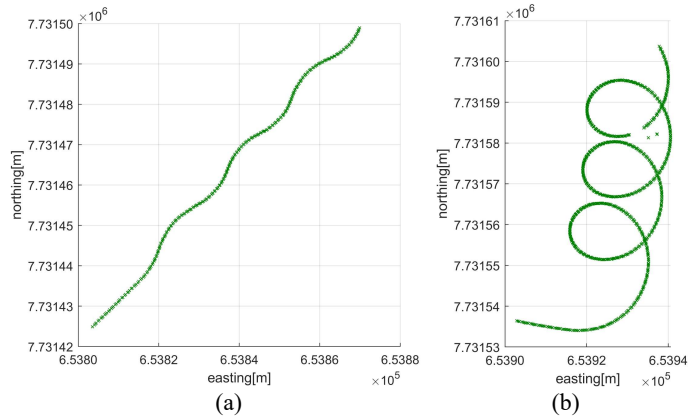


Fig.11. The measured position of the zigzag and port-turning maneuver. There exist outliers of measurements in the port-tuning maneuver.

In the zigzag maneuver, the predicted scaling factor α is depicted in Fig.12. It is evident that as the magnitude of $|y_r|$ increases, a comparatively higher α is computed using the trained GPR model. The adaptive tuning facilitated by this GPR model results in the scaling factor α tending to be larger when the ship executes a zigzag maneuver. This observation implies that the final estimates will assign greater importance to the measured data during the zigzag stage.

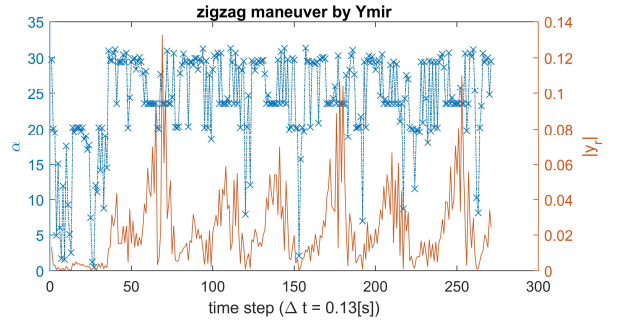


Fig. 12. $|y_r|$ and predicted α of the zigzag maneuver

The innovations of northing and easting (y_N & y_E) are illustrated in Fig.13. In the absence of adaptive tuning, the innovations exhibit significant fluctuations during the zigzag stage. Conversely, the adaptive tuning mechanism mitigates these fluctuations, resulting in lower innovations during the same stage. This indicates that with tuned Q , both the CMM and CTRA demonstrate higher accuracy compared to the same models with constant Q .

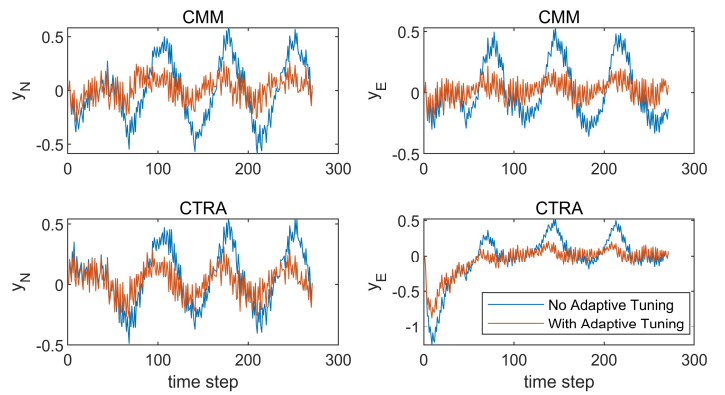


Fig. 13. The comparison between the y_N and y_E w/o adaptive tuning in the CMM and CTRA (zigzag maneuver).

The estimated velocities are presented in Fig.14-15. It is noticeable that velocities estimated with adaptive tuning exhibit a relatively faster reaction time when the ship receives new rudder orders. This attribute holds significance in real-time applications that necessitate swift responses to environmental changes.

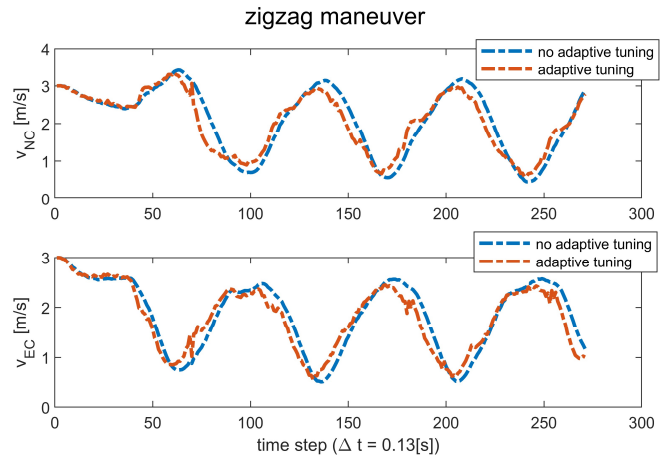


Fig. 14. Estimated velocities (v_{NC} & v_{EC}) from the CMM

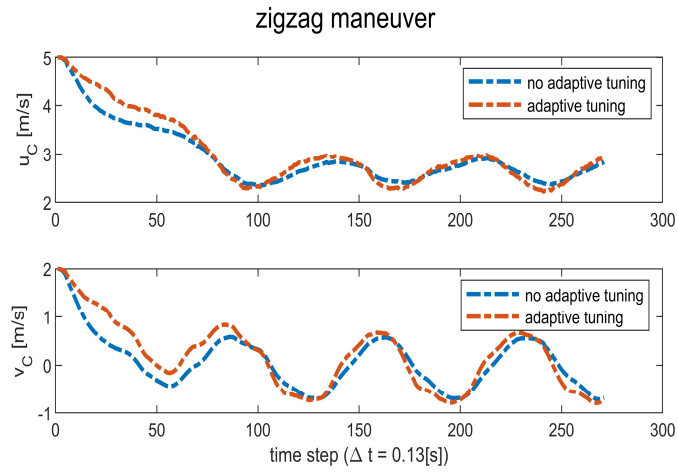


Fig. 15. Estimated velocities (u_C & v_C) from the CTRA

The computed α for the port-turning maneuver is depicted in Fig.16. It is evident that α tends to exhibit higher values once the ship initiates the turning process. The significant magnitude of $|y_r|$ during the turning stage suggests that the ship encounters disturbances more frequently than in the initial phase when executing a straight-line maneuver. These disturbances during the turning stage are attributed partly to the influence of a strong sea current, as evidenced by the measured positions indicating the ship's drift (Fig.11(b)).

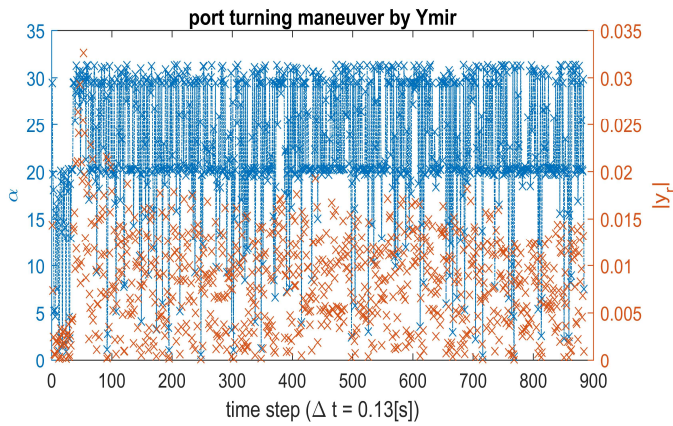


Fig. 16. $|y_r|$ and predicted α of the port turning maneuver

The innovations of northing and easting from the port turning maneuver are illustrated in Fig.17. Similar to the zigzag scenario, the innovations exhibit less fluctuation with the adaptive tuning mechanism. However, a significant deviation in the innovations is noticeable during time steps when abnormal measured positions are recorded. In such cases, the adaptive tuning of R is activated. The estimated positions and velocities are presented in Fig.18-20. It is observed that with the adaptive tuning of R , the posterior estimates rely more on the system models once abnormal measurements are detected. The estimated velocities with adaptive tuning appear smoother compared to those with constant Q and R .

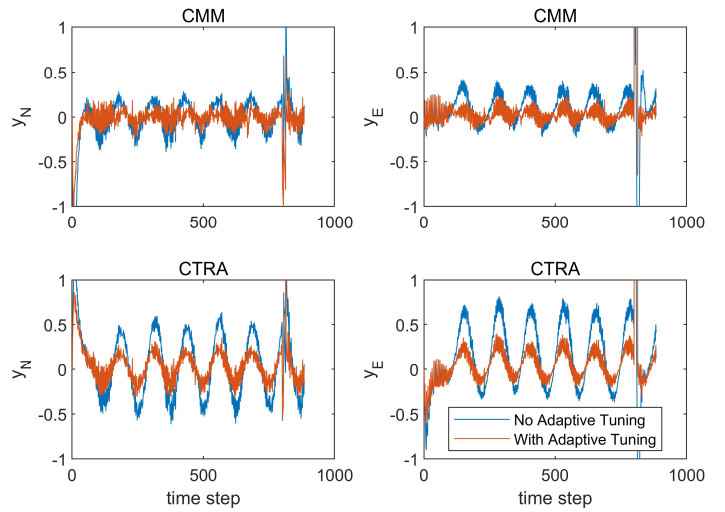


Fig. 17. The comparison between the y_N and y_E w/o adaptive tuning in the CMM and CTRA (port turning maneuver). The large value of innovations is caused by the outliers of measured positions.

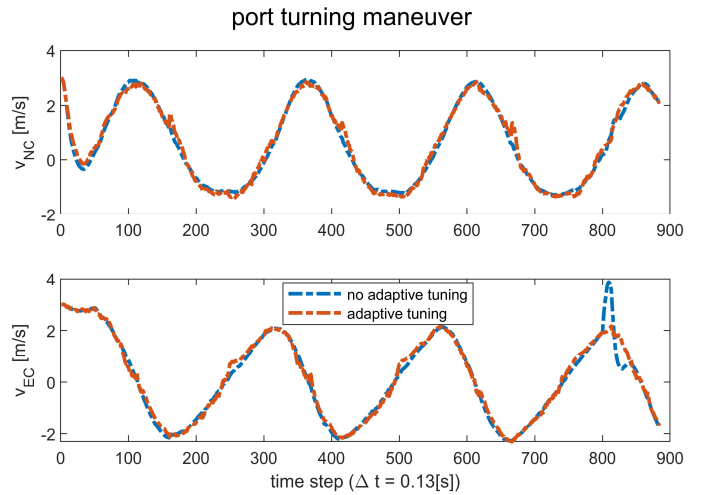


Fig. 18. Estimated velocities (v_{NC} & v_{EC}) from the CMM

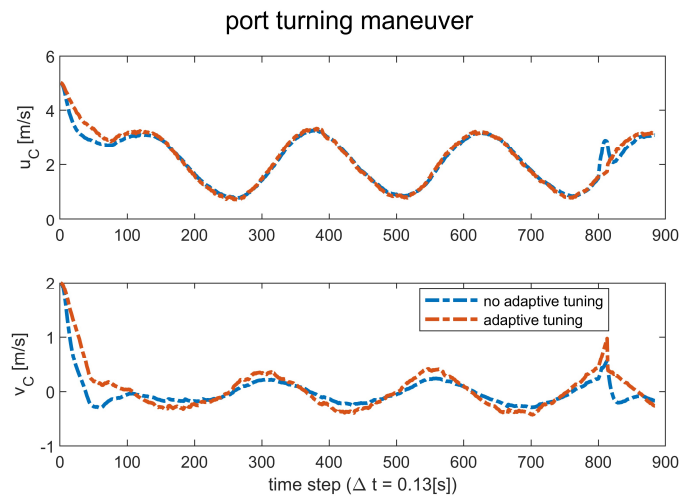


Fig.19. Estimated velocities (u_C & v_C) from the CTRA

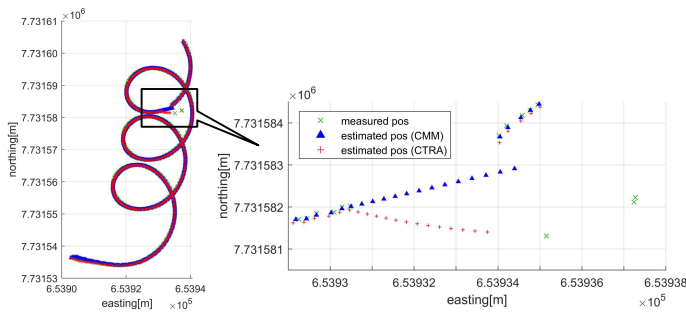


Fig.20. Estimated positions in the port turning maneuver. The time steps during which abnormal measurements occur are magnified for closer examination.

Additionally, it can be observed that the CMM exhibits greater robustness than the CTRA when confronted with abnormal measured positions. The positions estimated by the CMM appear smoother than those from the CTRA. The estimated sway velocity from the CTRA still displays discontinuous jumping. This indicates that the ship navigation states used in the CTRA can be more sensitive to measurement outliers.

CONCLUSIONS

An adaptive tuning mechanism is implemented in the KF-based state estimation, where the system models are generated by the kinematic motion models. Simulated maneuvers from the UiT bridge simulator are utilized to determine the optimal scaling factor for the system noise Q . Subsequently, a GPR model is trained by using the sampled simulated data. The sea-trial experiment data from the vessel 'Ymir,' comprising zigzag and port-turning maneuvers, is used to further evaluate the adaptive tuning mechanism. The results reveal that, with the adaptive tuning mechanism, the innovations in positions exhibited reduced fluctuations compared to positions estimated with constant Q and R . The estimated velocities adapt more swiftly to new rudder orders. In instances where the measured positions contained abnormalities, the adaptive tuning mechanism contributed to the enhanced smoothness of the estimated states.

In this research, the assessment of the adaptive tuning mechanism is constrained to relying solely on innovations due to the absence of actual ship navigation states. Consequently, the upcoming sea-trial experiment aims to collect a more diverse range of data from the installed onboard sensors through multiple trails so that more comprehensive evaluations by various criteria can be feasible. Additionally, the exploration of training a GPR model using datasets from the sea-trial experiment is under consideration. These datasets encompass unforeseen uncertainties stemming from the complex navigation environment.

ACKNOWLEDGEMENTS

This work has been conducted under the Autonomous ship Program in UiT-The Arctic University of Norway, which aims to develop the digital helmsman as a part of the ship intelligence to operate future vessels supported by the MARKOM II project under the project title "Onshore Operation Center for Remotely Controlled Vessels (OOC 2023)" under the contract number PMK-2022-10014.

REFERENCES

Almagbile, A., J. Wang and W. Ding (2010). "Evaluating the Performances of Adaptive Kalman Filter Methods in GPS/INS

Integration." *Journal of Global Positioning Systems* **9**.
 Alsuwaidan, B., J. Crassidis and Y. Cheng (2011). "Generalized Multiple-Model Adaptive Estimation using an Autocorrelation Approach." *Aerospace and Electronic Systems, IEEE Transactions on* **47**: 2138-2152.
 Andrew, G. and J. Gao (2007). Scalable training of L1-regularized log-linear models. *Proceedings of the 24th international conference on Machine learning*. Corvallis, Oregon, USA, Association for Computing Machinery: 33-40.
 Baybura, T., İ. Tiryakioglu, M. A. Uğur, H. İ. Solak and Ş. Şafak (2019). "Examining the Accuracy of Network RTK and Long Base RTK Methods with Repetitive Measurements." *Journal of Sensors* **2019**: 3572605.
 Efe, M., J. A. Bather and D. P. Atherton (1999). *An adaptive Kalman filter with sequential rescaling of process noise*. Proceedings of the 1999 American Control Conference (Cat. No. 99CH36251).
 Hu, C., W. Chen, Y. Chen and D. Liu (2003). "Adaptive Kalman Filtering for Vehicle Navigation." *Journal of Global Positioning Systems* **2**: 42-47.
 Kawase, K. (2013). *Concise Derivation of Extensive Coordinate Conversion Formulae in the Gauss-Krüger Projection*.
 Li, X. R. and V. P. Jilkov (2003). "Survey of maneuvering target tracking. Part I. Dynamic models." *IEEE Transactions on Aerospace and Electronic Systems* **39**(4): 1333-1364.
 Mazar, E., A. Averbuch, Y. Bar-Shalom and J. Dayan (1998). "Interacting multiple model methods in target tracking: a survey." *IEEE Transactions on Aerospace and Electronic Systems* **34**(1): 103-123.
 Ohhira, T., A. Shimada and T. Murakami (2021). "Variable Forgetting Factor-Based Adaptive Kalman Filter With Disturbance Estimation Considering Observation Noise Reduction." *IEEE Access* **9**: 100747-100756.
 Perera, L. (2019). "Deep Learning towards Autonomous Ship Navigation and Possible COLREGs Failures." *Journal of Offshore Mechanics and Arctic Engineering*.
 Perera, L. P. (2017). "Navigation vector based ship maneuvering prediction." *Ocean Engineering* **138**: 151-160.
 Thombre, S., Z. Zhao, H. Ramm-Schmidt, J. M. V. García, T. Malkamäki, S. Nikolskiy, T. Hammarberg, H. Nuortie, M. Z. H. Bhuiyan, S. Särkkä and V. V. Lehtola (2022). "Sensors and AI Techniques for Situational Awareness in Autonomous Ships: A Review." *IEEE Transactions on Intelligent Transportation Systems* **23**(1): 64-83.
 Wang, Y., L. P. Perera and B.-M. Batalden (2023). "Kinematic motion models based vessel state estimation to support advanced ship predictors." *Ocean Engineering* **286**: 115503.
 Wu, M., L. Qin, G. Wu, Y. Huang and C. Shi (2021). "State of Charge Estimation of Power Lithium-ion Battery Based on a Variable Forgetting Factor Adaptive Kalman Filter." *Journal of Energy Storage* **41**: 102841.